AIAA JOURNAL
Vol. 34, No. 6, June 1996

Two-Layer Approximate Boundary Conditions for Large-Eddy Simulations

Elias Balaras* and Carlo Benocci†
von Kármán Institute for Fluid Dynamics, 1640 Rhode St Génèse, Belgium
and
Ugo Piomelli‡
University of Maryland, College Park, Maryland 20742

A new method to model the effect of the solid boundaries on the rest of the flowfield in large-eddy simulations is proposed. The filtered Navier–Stokes equations are solved up to the first computational point. From there to the wall, a simplified set of equations is solved, and an estimate of the instantaneous wall shear stress required to impose boundary conditions is obtained. Computations performed for the plane channel, square duct, and the rotating channel flow cases gave improved results compared with existing models. The additional computing time required by the model is on the order of 10–15% of the overall computing time. The mean flow quantities and low-order statistics, which are of primary interest in engineering calculations, are in very good agreement with the reference data available in the literature.

I. Introduction

LARGE-EDDY simulation (LES) is based on the decomposition of turbulent quantities into a resolved large-scale component and an unresolved part due to scales smaller than a typical size defined by the numerical resolution. Transport equations for the large-scale quantities are solved, in which the effect of the small subgrid scales is modeled. Since the small scales tend to be more homogeneous and isotropic than the large ones and less affected by the boundary conditions, it is assumed that the subgrid scale (SGS) terms that appear in the equations for the resolved scales can be modeled by simple eddy-viscosity models. Thus, LES requires a much reduced computational effort compared with direct simulations (DNS), in which all scales of motion are resolved: the number of grid points required by a DNS is proportional to $Re^{9/4}$ (and the cost to Re^3); in an LES, on the other hand, when the cutoff between the large and the small scales is in the inertial region of the spectrum, the resolution (and hence the cost) becomes nearly independent of the Reynolds number.

The cost of an LES calculation, however, depends on the Reynolds number if a solid surface is present, since in that case even the largest scales of motion depend on the Reynolds number. Chapman[1] estimated that the resolution required to resolve the outer layer of a growing boundary layer is proportional to $Re^{0.4}$, whereas for the viscous sublayer (which, in aeronautical applications, only accounts for approximately 1% of the boundary-layer thickness) the number of points needed increases at least like $Re^{1.8}$. Thus, although LES can give some improvement over DNS and can be extended to flows at Reynolds numbers at least one order of magnitude higher than DNS at a reasonable cost, its application to engineering flows remains prohibitively expensive.

One way to overcome this problem is to use approximate wall boundary conditions similar to the wall functions employed in Reynolds stress models. The basic assumption behind this approach is that the interaction between the modeled near-wall region and the resolved outer region is weak. Despite the large effort undertaken over the past decades in understanding the dynamics of the viscous near-wall region, which are directly related to the dynamics of organized coherent vortices present in the region (see Robinson[2] for a review), little information became available on the validity of the preceding assumption. Some support, however, can be obtained from a recent paper of Brooke and Hanratty,[3] in which the way the near-wall vortices are born is investigated, utilizing DNS databases for a turbulent channel flow. An important finding is that the flow structures in the viscous wall region, which are responsible for most of the shear stress production, regenerate themselves. No interaction with the outer layer structures was detected.

Approximate boundary conditions available currently assume that the dynamics of the wall layer are universal and that some generalized law-of-the-wall can be imposed. The laws-of-the-wall imposed so far have been quite simple, usually based on the logarithmic velocity profile.

Deardorff,[4] in his channel flow computations, forced the existence of a logarithmic layer and made the additional assumption that the turbulent fluctuations be isotropic:

$$\frac{\partial^2 \bar{u}}{\partial z^2} = -\frac{1}{\kappa(\Delta z/2)^2} + \frac{\partial^2 \bar{u}}{\partial y^2} \tag{1}$$

$$\frac{\partial^2 \bar{v}}{\partial z^2} = \frac{\partial^2 \bar{v}}{\partial x^2} \tag{2}$$

where x or x_1 indicates the streamwise direction, y or x_2 the spanwise direction, and z or x_3 the wall-normal direction; u, v, and w (or u_1, u_2, and u_3) are the velocity components in the three coordinate directions, respectively, and an overbar denotes a filtered (or large-scale) quantity. In this and in all other cases discussed in this work, the no-transpiration condition ($\bar{w} = 0$ at the wall) is applied on the wall-normal velocity component.

For the same flow, Schumann[5] used conditions that related the wall stress to the velocity in the core by

$$\tau_{13} = \frac{\langle \tau_w \rangle}{\langle \bar{u}(x, y, z_2) \rangle} \bar{u}(x, y, z_2) \tag{3}$$

$$\tau_{23} = \frac{1}{Re_\tau} \frac{\bar{u}(x, y, z_2)}{\Delta z/2} \tag{4}$$

These equations, in which z_2 indicates the first grid point off the solid wall, impose that the wall stress is proportional to the velocity at the first point (both in the streamwise and spanwise directions). The mean stress $\langle \tau_w \rangle$ can be known for a given pressure gradient or can be calculated iteratively by requiring that the plane-averaged velocity at the first grid point, $\langle \bar{u}(x, y, z_2) \rangle$, satisfy the logarithmic

Received March 29, 1995; revision received Aug. 8, 1995; accepted for publication Aug. 10, 1995.

*Research Fellow, Environmental and Applied Fluid Dynamics Department, Chaussée de Waterloo 72.
†Professor, Environmental and Applied Fluid Dynamics Department, Chaussée de Waterloo 72.
‡Associate Professor, Department of Mechanical Engineering. Senior Member AIAA.

law.[6] Grötzbach[6] used a similar approach to calculate turbulent flows with heat transfer.

Mason and Callen[7] required the logarithmic law to be satisfied locally and instantaneously at the first grid point. This assumption is based on local equilibrium of the near-wall region that depends on the size of the averaging volume (the grid cell) and may not be valid for flows more complex than the standard boundary layer or plane channel.

Piomelli et al.[8] applied conditions similar to Eqs. (3) and (4); however, they required the wall stress to be correlated to the instantaneous velocity some distance downstream of the point where the wall stress is required, to take into account the inclination of the elongated structures in the near-wall region:

$$\tau_{13}(x, y, 0) = \frac{\langle \tau_w \rangle}{\langle \bar{u}(x, y, z_2) \rangle} \bar{u}(x + \Delta_s, y, z_2) \tag{5}$$

$$\tau_{23}(x, y, 0) = \frac{\langle \tau_w \rangle}{\langle \bar{u}(x, y, z_2) \rangle} \bar{v}(x + \Delta_s, y, z_2) \tag{6}$$

where Δ_s is a streamwise displacement; its optimum value can be obtained from DNS or experimental data and is approximately $\Delta_s = z_2 \cot 8$ deg for $30 < z_2^+ < 50$, and $\Delta_s = z_2 \cot 13$ deg for larger distances. The plane-averaged wall stress is obtained solving iteratively a generalized law-of-the-wall that is also valid for flows with transpiration. These changes yielded improved results with respect to Schumann's original model.[5] This model has been used recently by Balaras et al.[9] to study the flow in a plane channel at high Reynolds number in conjunction with the dynamic SGS model, with results in excellent agreement with experimental and DNS data.

An alternative class of approximate boundary conditions that has shown much promise in preliminary studies is based on the use of linear stochastic estimation (LSE) to obtain the wall stress. This technique has been applied successfully[10,11] to the study of plane channel flow, giving very accurate prediction of the statistics; however, it requires that the full two-point correlation tensor be known a priori (i.e., from experiment or previous DNS). Although this requirement might seem unrealistic, recent results indicate that if the correlations are known at a given Reynolds number, scaling arguments[12] may be invoked to use them at different Reynolds numbers. The model is yet to be extended to more complex configurations.

In this paper a different approach will be proposed. The filtered Navier–Stokes equations are solved in the core of the flow, whereas from the first grid point to the wall, a simpler set of equations (the boundary-layer equations) are solved numerically, and the effect of all scales of motion is modeled.

A similar zonal approach is implicitly used in currently available approximate boundary conditions, when some form of the logarithmic layer is imposed. This is equivalent to an approximate integration of the boundary-layer equations with a mixing length model used to parameterize the effect of the interaction between the inner and the outer layer.

Even in well-resolved LES, especially at high Reynolds numbers, an approach of this type is followed implicitly: the grid in the near-wall region is extremely anisotropic, with aspect ratios as large as 160:30:1 near the wall (respectively, in the streamwise, spanwise, and wall-normal directions), gradually increasing to 160:30:80 in the channel center (see Ref. 13). Such grids cannot resolve the spanwise (and, less importantly, the streamwise) velocity gradients with the same accuracy as the normal ones, and it can be argued that, in the near-wall region, the thin shear layer (TSL) equations are actually solved, whereas the SGS model is used to parameterize the effect of all unresolved scales, including, to some extent, the near-wall turbulence structures.

The results of Piomelli[13] support this line of reasoning. In calculations of plane channel flow at $Re_\tau = 1 \times 10^3 - 2 \times 10^3$ based on shear velocity and channel halfwidth ($Re_b = 4.3 \times 10^4 - 8.5 \times 10^4$, based on the bulk velocity and channel height), he observed that as the grid was coarsened, the streaky structures in the near wall were captured less and less accurately. Although the resolution in the wall layer was marginal, towards the channel centerline a decay of several orders of magnitude was observed in the spectra, indicating that the cutoff between the large and small scales was in the dissipation range, so that the calculation was effectively a DNS. In the logarithmic layer, on the other hand, the cutoff was in the inertial range. In other words, the actual Navier–Stokes equations were solved at the channel centerline, the filtered Navier–Stokes equations in the logarithmic region, and some form of the filtered TSL equations near the wall. In the outer region, the SGS model gave negligible contribution to the stresses, whereas near the wall it adjusted itself to the coarseness of the mesh by providing more backscatter (and hence, less dissipation) to account for the energy production of the unresolved scales.

The mathematical formulation of the problem, including the wall layer modeling approach, will be presented in the next section. Then the proposed method will be applied to the calculation of three test problems: the flow in a plane channel, in a square duct, and in a rotating channel. The results of the new method will be compared with those obtained using standard approximate boundary conditions (and with experimental and numerical data) in Sec. III. Conclusions and recommendations for future work will be made in Sec. IV.

II. Mathematical Formulation

In LES, the large-scale velocity field can be obtained from the solution of the filtered Navier–Stokes equations, where scales smaller than the grid size are modeled. The filtering operation, which defines the large-scale variables (denoted by overbar), can be written as

$$\bar{f}(x) = \frac{1}{\bar{\Delta}_1 \bar{\Delta}_2 \bar{\Delta}_3} \int_D f(x')\, dx' \tag{7}$$

where D is the control volume (the finite difference cell). The preceding is essentially a top-hat filter in physical space and is applied implicitly by the finite difference operators.

Applying the filtering operation to the incompressible Navier–Stokes and continuity equations yields the filtered equations of motion

$$\frac{\partial \bar{u}_i}{\partial t} + \frac{\partial}{\partial x_j}(\bar{u}_i \bar{u}_j) = -\frac{1}{\rho}\frac{\partial \bar{p}}{\partial x_i} - \frac{\partial \tau_{ij}}{\partial x_j} + \nu \frac{\partial^2 \bar{u}_i}{\partial x_j \partial x_j} \tag{8}$$

$$\frac{\partial \bar{u}_i}{\partial x_i} = 0 \tag{9}$$

The effect of the small scales upon the resolved part of turbulence appears in the SGS stress term, $\tau_{ij} = \overline{u_i u_j} - \bar{u}_i \bar{u}_j$, which is modeled by the dynamic eddy viscosity model,[14] which assumes an eddy viscosity representation for the small scales[15]:

$$\tau_{ij} - (\delta_{ij}/3)\tau_{kk} = -2\nu_T \bar{S}_{ij} = -2C(x, t)\bar{\Delta}^2 |\bar{S}| \bar{S}_{ij} \tag{10}$$

in which δ_{ij} is Kronecker's delta, and $\bar{\Delta}$ is the filter width $\bar{\Delta}^3 = \bar{\Delta}_1 \bar{\Delta}_2 \bar{\Delta}_3$; $|\bar{S}| = (2\bar{S}_{ij}\bar{S}_{ij})^{1/2}$ is the magnitude of the large-scale strain rate tensor

$$\bar{S}_{ij} = \frac{1}{2}\left(\frac{\partial \bar{u}_i}{\partial x_j} + \frac{\partial \bar{u}_j}{\partial x_i}\right) \tag{11}$$

and the trace of the SGS stresses is included in the pressure term. To determine the coefficient C, the least-squares minimization procedure proposed by Lilly[16] is adopted here, and the coefficient is given by

$$C = -\frac{1}{2}\frac{\langle \mathcal{L}_{ij} M_{ij} \rangle}{\langle M_{ij} M_{ij} \rangle} \tag{12}$$

where

$$\mathcal{L}_{ij} = \widehat{\bar{u}_i \bar{u}_j} - \hat{\bar{u}}_i \hat{\bar{u}}_j, \qquad M_{ij} = \hat{\Delta}^2 |\hat{\bar{S}}| \hat{\bar{S}}_{ij} - \bar{\Delta} \widehat{|\bar{S}| \bar{S}_{ij}}$$

and $\hat{}$ denotes a quantity filtered using the test filter $\hat{G}$ (with filter width $\hat{\Delta} = 2\bar{\Delta}$). To avoid ill-conditioning and mathematical inconsistencies, averaging of the coefficient over homogeneous directions (denoted here by $\langle \cdot \rangle$) is performed.

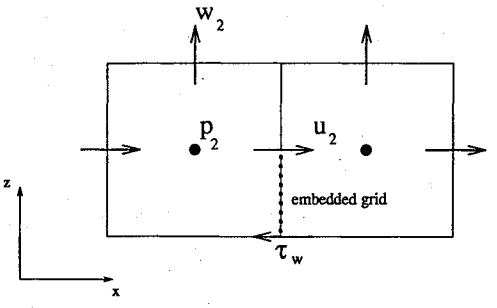

Fig. 1 Two-dimensional representation of a wall cell. The embedded grid and the location of the filtered variables are shown.

Equations (8) and (9) are integrated in time using a fractional-step method. All space derivatives are approximated by second-order-accurate central differences on a staggered mesh. The Poisson equation for the pressure is solved using a direct Poisson solver based on fast Fourier transforms.[17] Both advective and diffusive terms are treated explicitly using an Adams–Bashforth scheme. Periodic boundary conditions are used in the streamwise direction for all calculations and in the spanwise direction for the channel flow simulations. Further discussion of the numerical scheme and of the implementation of the dynamic model on the staggered mesh can be found in Ref. 9.

At the solid boundaries, the zonal treatment described in the Introduction is performed. The filtered Navier–Stokes equations (8) and (9) are solved up to the first grid point. From the first grid point to the wall, a refined mesh is embedded into the main one (see Fig. 1) and a simplified equation, based on the two-dimensional boundary-layer equations, is solved:

$$\frac{\partial \bar{u}_i}{\partial t} + \frac{\partial}{\partial x_1}(\bar{u}_1\bar{u}_i) + \frac{\partial}{\partial x_n}(\bar{u}_n\bar{u}_i) = -\frac{\partial \bar{p}}{\partial x_i} + \frac{\partial}{\partial x_n}\left[(\nu + \nu_t)\frac{\partial \bar{u}_i}{\partial x_n}\right] \tag{13}$$

where the index n denotes the direction normal to the boundary. When the solid boundary is in the $x-y$ plane, Eq. (13) is solved for $i = 1, 2$, whereas for a boundary in the $x-z$ plane, it is solved for $i = 1, 3$. In both cases the wall-normal component u_n is obtained by applying mass conservation.

With this approach, the inner part of the boundary layer is assumed to behave like a Stokes layer driven by the outer (core) flow. The eddy viscosity plays a more significant role in the near-wall region than in the core of the flow, since near the boundary it must represent the effect of all of the scales of motion, whereas in the core it only represents the effect of the subgrid scales. Consequently, a more sophisticated parameterization might be desirable, especially in complex configurations. In the present work, which focuses on the feasibility of the two-layer approach, however, a very simple mixing-length model is used to represent ν_t:

$$\nu_t = (\kappa z)^2 D(z)|S| \tag{14}$$

where κ is the von Kármán constant, z the distance from the solid boundary, $|S|$ is the magnitude of the total strain rate, and D is a damping function used to ensure the correct limiting behavior for ν_t. An expression proposed by Piomelli et al.[8] is adopted here:

$$D(z) = \{1 - \exp[-(z^+/A^+)^3]\} \tag{15}$$

where $A^+ = 25$.

Equation (13) is discretized using second-order finite differences. The diffusive terms are treated implicitly by a Crank–Nicolson scheme to avoid stability restrictions, whereas the advective terms are treated explicitly. The pressure term appears as a source term in the discrete equations, since it is assumed that $\partial \bar{p}/\partial x_n = 0$. The solution gives velocity profiles for the streamwise and spanwise components at each time step, which provide the wall stress required to solve the filtered Navier–Stokes and continuity equations (8) and (9) at the first outer flow point.

With this treatment the computation of the wall shear stress is decoupled from the actual LES, as it is done in the case of currently available approximate wall boundary conditions, (the shifted model for example). The link with the actual LES is the velocity and pressure field at the first inner computational point, which provides the upper boundary condition for the domain where the refined grid is embedded and the model equation is solved. No-slip boundary conditions are applied at the solid wall. As a result continuity of the velocity fields obtained with the two different set of equations at the interface is forced. Continuity of the shear stress is not necessary with the present approach: this is because the derivative of the shear stress is evaluated on the actual LES grid, where (in the framework of central finite differences) the total stress is assumed to be only piecewise constant. In practice, however, the shear stress is found to be continuous.

III. Results and Discussion

To investigate the range of applicability of the proposed model and evaluate its accuracy, three different problems were investigated: the flow in a plane channel, the flow in a straight square duct, and the flow in a channel subjected to system rotation. For the first case a variety of accurate DNS, well-resolved LES, and experimental data are available for a range of Reynolds numbers. Furthermore, very good results have been obtained with currently available approximate wall boundary conditions. The accuracy of the two-layer model in comparison with existing models as well as the influence of several parameters can be examined. In the last two flow cases the robustness and the accuracy of the model can be investigated for more complex configurations. The initiation of the secondary flow in the square duct case and the presence of system rotation in the rotating channel flow case can decrease the accuracy of existing models. The assumption of the existence of a logarithmic layer is not valid and the extra empirical parameters required (shift angle for example) are not available for such cases.

A summary of all cases and calculation parameters considered is given in Table 1 (where the Reynolds number $Re_\tau = u_\tau \nu/\delta$ is based on the friction velocity u_τ and channel or duct half-width δ, and the rotation number $Ro_b = 2\delta\Omega/U_b$ is based on the bulk velocity of the flow U_b). The equations were integrated in time until steady state was reached. Statistics were accumulated over 4–8 units (tu_τ/δ). Further integration in time was found to have negligible influence on the mean flow quantities and turbulent statistics.

A. Plane Channel Flow

For the plane channel flow case three computations were performed at two different Reynolds numbers (cases 1–3 in Table 1). The size of the computational box is $4\pi\delta \times \pi\delta \times 2\delta$ for case 1 and $2.5\pi\delta \times 2\delta \times 2\delta$ for cases 2 and 3. Case 1 is a low-Reynolds-number case for which reliable DNS data[18] are available. The location of the first point close to the solid boundary is $z^+ \simeq 11$. A uniform grid with 21 points is used from the first computational point to the wall for the solution of the model equation (13). Cases 2 and 3 are high-Reynolds-number cases that can be used to test the dependence of the solution on the location of the first grid point. For this reason the resolution in the outer layer is approximately the same: 32 equally spaced points are used in the wall normal direction for case 2, resulting in $\Delta z^+ = 125$, whereas 42 unequally spaced points are used for case 3, resulting in $125 > \Delta z^+ > 75$. The location of the first grid point is $z^+ \simeq 65$ for case 2 and $z^+ \simeq 35$ for case 3. For

Table 1 Summary of the computations

Case	Flow type	Re_τ	Ro_b	Grid size	Embedded grid
1	Plane channel	2×10^2	0.0	$42 \times 22 \times 20$	21
2	Plane channel	2×10^3	0.0	$42 \times 34 \times 34$	41
3	Plane channel	2×10^3	0.0	$42 \times 34 \times 42$	25
4	Square duct	1.125×10^3	0.0	$82 \times 34 \times 34$	21
5	Rotating channel	2×10^2	0.069	$42 \times 34 \times 20$	21
6	Rotating channel	2×10^2	0.144	$42 \times 34 \times 20$	21
7	Rotating channel	2×10^2	0.210	$42 \times 34 \times 20$	21

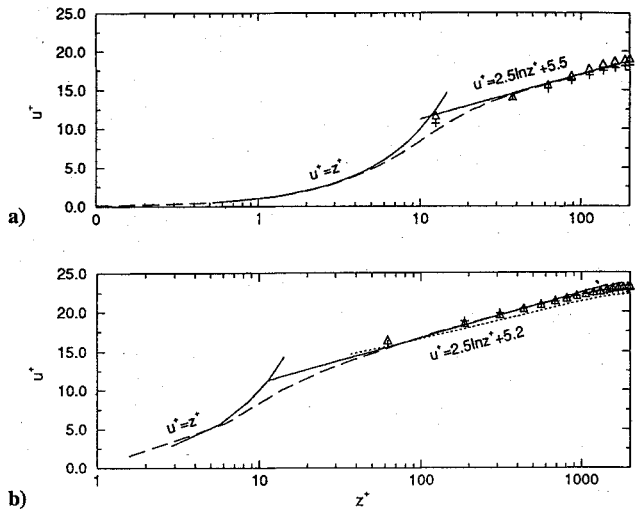

Fig. 2 Plane channel flow; mean velocity profiles in wall coordinates: a) $Re_\tau = 200$: ——, DNS[18]; case 1: +, two-layer model, △, shifted model; and b) $Re_\tau = 2000$: - - -, resolved LES[13]; case 2: +, two-layer model, △ shifted model; case 3: ....., two-layer model.

the latter case the number of grid points used in the near-wall region is reduced to 25 to solve the model equation with the same accuracy as for case 2. For the high Reynolds number, experimental[19] and LES data[13] with the wall layer resolved and no-slip boundary conditions applied on the solid wall are available for comparisons. For cases 1 and 2 the computations were repeated using the shifted model, Eqs. (5) and (6). Following Piomelli et al.[8] the streamwise displacement was set to $\Delta_s = z_2 \cot 8$ deg.

The mean streamwise velocity profiles compared with numerical and experimental data are shown in Fig. 2. The agreement with the data is very good and little differences can be observed between the two models. For case 1 the two-layer model performs better than the shifted one, which tends to underpredict the wall stress, leading to higher velocities across the channel. For case 2 the differences are negligible. This is probably because for case 1 the first point close to the solid wall lies in the buffer layer ($z^+ \simeq 11$), whereas for case 2 it is inside the logarithmic layer ($z^+ \simeq 65$). The shifted model and all similar models operate better when the first computational point is well inside the logarithmic layer ($z^+ > 20$); for smaller distances a more general form of the law-of-the-wall must be used to improve the prediction of the wall stress τ_w. In general, the two-layer model was found to be insensitive to the value of z^+ and in all cases the predicted averaged wall stress is close to the expected value.

Profiles of turbulent intensities are given for $Re_\tau = 2 \times 10^2$ and 2×10^3 in Figs. 3 and 4, respectively. The present computations agree well with the data, and the differences between the two models are marginal. For both Reynolds numbers the normal turbulent intensities are underpredicted in the wall vicinity. This is a common problem with LES calculations, probably because the modeled small scales of motion have a considerable contribution to the wall normal fluctuations, whereas here only the resolved part of the stresses is shown. In general turbulent intensities are not very sensitive to the wall model used and its influence is restricted to the first few points in the wall proximity. Small improvements that can be observed when the two-layer model is used are due to a better estimation of the wall stress used to normalize the data.

In Figs. 2 and 4 the mean velocity profiles and turbulent intensities for case 3 are also shown. As already remarked, these cases only differ in the distance of the first grid point from the solid boundary, and all other parameters have been kept approximately the same. For both mean velocity and turbulent intensity profiles the differences are marginal, demonstrating that the accuracy of the solution is independent from the location of the first grid point, at least for $z_2^+ < 100$.

In Fig. 5 the mean streamwise velocities predicted by the model equation in the wall layer are shown. The agreement with the data is good. In Fig. 6a profiles of the mean shear stress $\langle \tau_{13} \rangle$ across the

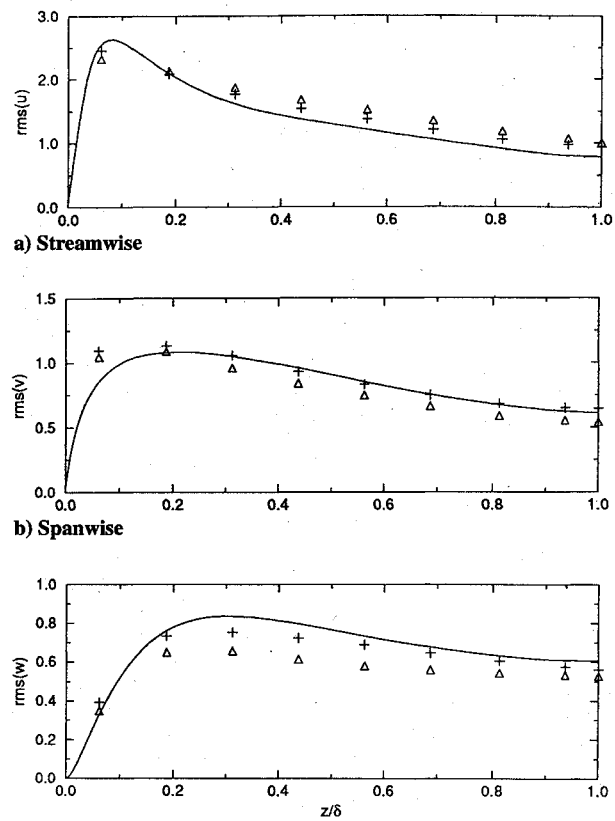

Fig. 3 Plane channel flow; turbulence intensities in outer coordinates for $Re_\tau = 200$: ——, DNS[18]; case 1: +, two-layer model; and △, shifted model.

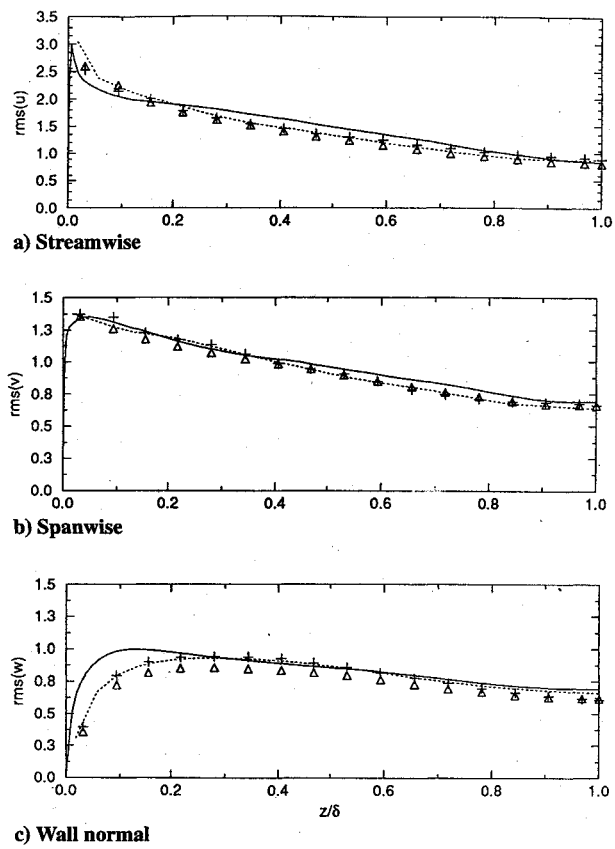

Fig. 4 Plane channel flow; turbulence intensities in outer coordinates for $Re_\tau = 2000$: ——, resolved LES[13]; case 2: +, two-layer model; and △ shifted model; and case 3: ....., two-layer model.

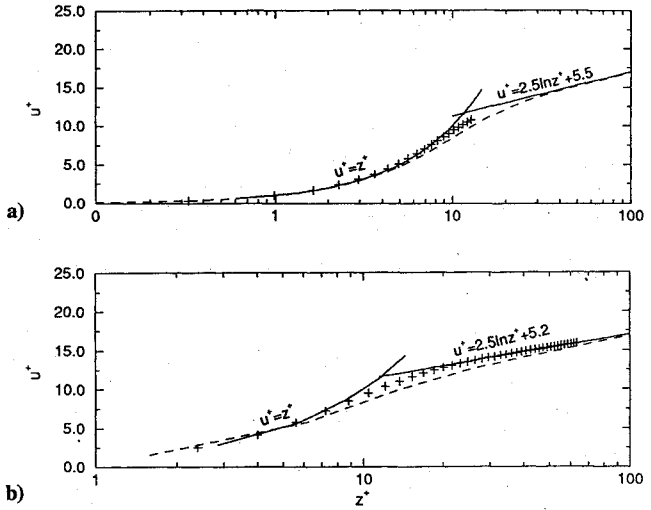

Fig. 5 Plane channel flow; mean velocity profiles in the wall layer predicted by the model equation: a) case 1: +, wall layer model; - - -, DNS[18]; and b) case 2: +, wall layer model; - - -, resolved LES.[13]

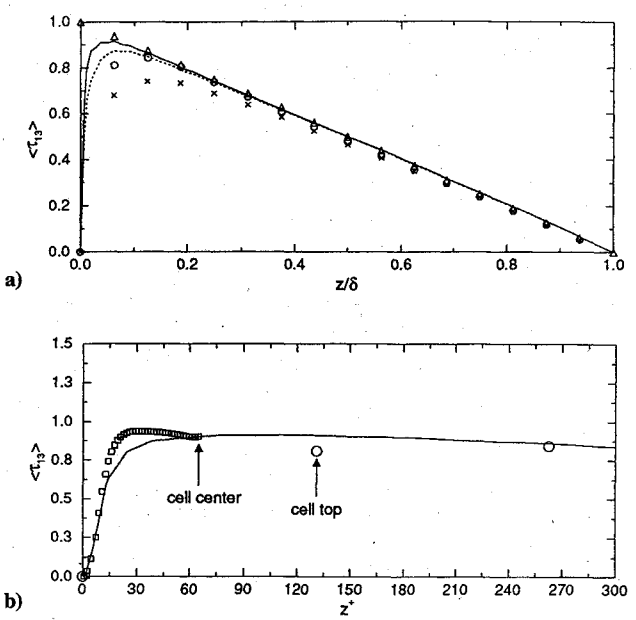

Fig. 6 Shear stress distribution in the plane channel flow for case 2: a) outer layer: lines represent the resolved LES data[13], symbols are the present computation: ×, - - -, large-scale; ○,——, large-scale+SGS; and △ total; and b) inner layer: ——, large-scale+SGS[13]; □, large-scale+SGS predicted by the wall model; ○, large-scale+SGS in the outer layer computation.

channel are shown for case 2. In general the agreement with the reference data is very good. Only at the first cell close to the solid surface the predicted value of resolved + SGS stress is lower than in the reference simulation, resulting in a higher velocity gradient at the first grid point (see Fig. 2). A possible cause for this error could lie in the fact that at the first grid cell the test-filtered strain rates required in the computation of the model coefficient C are essentially extrapolated from the interior,[9] which may affect the accuracy of the SGS model. Errors due to the wall model, however, do not propagate into the core of the flow.

The mean shear stress predicted by the model equation (14) in the near-wall region (Fig. 6b) is in acceptable agreement with the resolved LES data even near the wall, despite the fact that a very simple turbulence model is used. It is also worthwhile to mention that, although continuity of the stresses is not required, in practice one observes a smooth transition from the inner to the outer layer, especially at high Reynolds numbers.

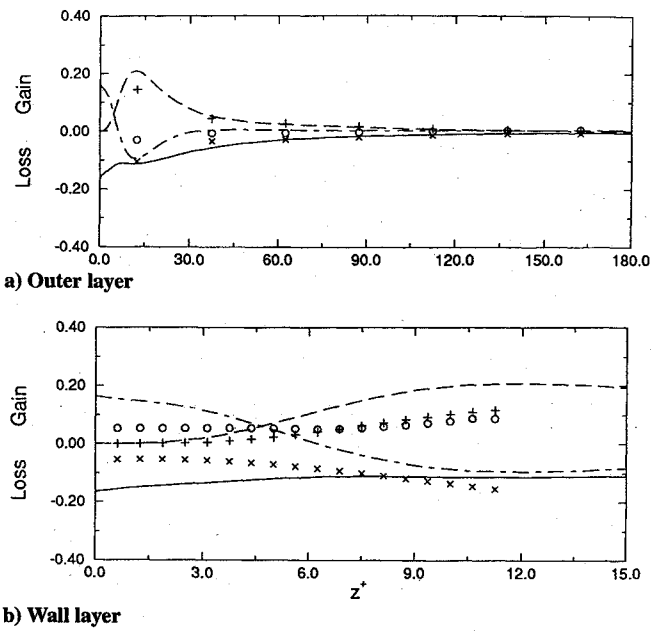

Fig. 7 Turbulent kinetic energy balance terms for Case 1. Lines are DNS data from Mansour et al.[20] and symbols are computed terms: - - - - +, production; ——×, dissipation (viscous+SGS); and —·—○, diffusion (viscous+pressure+turbulent+SGS).

In Fig. 7 the computed terms in the turbulent kinetic energy balance equation in the outer and inner layers are shown, compared with the DNS data reported in Mansour et al.[20] In the computed dissipation and diffusion terms the SGS contributions have been added. In the outer layer (Fig. 7a) the agreement is very good, indicating that the SGS model represents adequately the energy transfer between resolved and modeled scales. In general the outer layer is approximately in equilibrium (production and dissipation are dominant terms and roughly balance each other, whereas the sum of the diffusive terms is zero).

In the near-wall region, however, the exact production goes to zero and viscous dissipation is balanced by diffusion, which is now a significant term. The simple equilibrium-based model used in this region in this preliminary calculation cannot predict such effects correctly: the globally energy-conserving nature of the algorithm forces the diffusion term to have an unphysical behavior to balance the incorrectly predicted production and dissipation. It must, however, be remarked that in the present study the purpose of the inner layer calculation is only to provide the correct value of the wall stress, and this appears to be less sensitive to modeling errors introduced by the turbulence model in the near-wall region and is predicted with a fair degree of accuracy (see Fig. 5). In general, simple mixing length models have been found to result in satisfactory prediction of the mean velocity profiles (and therefore of the wall stress) in the wall region in a variety of flows,[21] despite their inability to predict correctly the energy exchange in this region. In regions of strong adverse pressure gradients or recirculating flow, however, their use appears to be more problematic. In such a case one-equation treatments could result in marked improvements of the prediction of the near-wall behavior.[22]

The additional CPU time required by the proposed model depends on the number of points used on the embedded mesh. Compared with the shifted model, it is approximately 10% more for case 1 and 15% more for case 2. This is still one order of magnitude smaller than the CPU time required by a resolved LES in which the exact no-slip boundary conditions are applied on solid walls. In general, the simulations reported in this study never required more than 10 CPU hours on fast desktop workstations, demonstrating the feasibility of LES as a tool for computations of engineering interest.

B. Square Duct Flow

In a square duct, secondary flow occurs in the transverse planes of the duct, which arises due to the anisotropy and inhomogeneity

of the Reynolds stresses. Speziale[23] has shown analytically that the secondary flow in ducts with noncircular cross sections originates from the fact that the axial mean velocity gives rise to a nonzero difference in the transverse normal Reynolds stresses responsible for the production of axial mean vorticity. The preceding argument is also supported by the experimental findings of Brundrett and Baines[24]; however, Gessner[25] in his experimental investigation reported that the gradients of turbulent shear stresses normal to the corner bisector play an important role in the generation of secondary flow, and he suggested that the mechanisms responsible for the production of the mean streamwise vorticity are not necessarily initiating the secondary motions. Although the secondary flow is very small in magnitude (2–3% of the bulk velocity), it has a significant effect on the overall flow structure. Gavrilakis[26] found that the mean streamwise velocity along a line of symmetry normal to the wall exhibits a logarithmic region of the form: $u^+ = 3.2\ln z^+ + 3.9$. These constants are quite different from the standard values. In the corner regions the influence of the secondary flow is much stronger and the mean streamwise velocity does not exhibit a logarithmic region, whereas deflection points can be observed in the profiles. Consequently, the use of currently available approximate wall boundary conditions is impractical and could introduce considerable inaccuracies.

A high-Reynolds-number case is considered for this flow type. The calculation parameters are summarized in Table 1 (case 4). The corresponding Reynolds number based on the bulk velocity U_b and the hydraulic diameter is 4.2×10^4. The size of the computational box was taken equal to $5.5\pi\delta \times 2\delta \times 2\delta$. This streamwise length was found to be sufficient to contain the largest structures present in the flow by a posteriori examination of the two point correlations.

In Fig. 8, isolines of the mean streamwise velocity and velocity vectors of the mean secondary flow are shown at a cross section. Although some asymmetry in the results is present, the main flow features are evident. In the following comparisons, all quantities will be averaged over the four quadrants.

The computation of case 4 was repeated using the shifted model, Eqs. (5) and (6). The streamwise displacement Δ_s was set to zero due the lack of available empirical information. The standard law-of-the-wall was used to obtain $\langle u_\tau \rangle$ with the streamwise line average of u as an input. The distribution of the predicted local wall shear stress τ_w normalized with the average wall stress $\langle \tau_w \rangle$ along the lower duct wall is given in Fig. 9. The measured values in Refs. 27 and 28 at comparable Reynolds numbers ($Re_b = 5 \times 10^4$ and 3.4×10^4, respectively) are also included. The wall shear stress predicted by the proposed model agrees well with the reference data; it follows closely the measured values with a midwall value of $1.005\langle \tau_w \rangle$. The shifted model also agrees with the experimental data in the midwall area, although $\tau_w/\langle \tau_w \rangle$ is somewhat lower than the experimental data. As the corner region is approached, the error increases and the predicted value of the wall stress is approximately 10% higher than the reference value, due to the assumption of the existence of a logarithmic layer.

In Fig. 10, mean streamwise velocity profiles normalized by U_b are given along the normal wall bisector. The agreement with the reference data is very good; the differences between the two models is small, probably because the shifted model in this region does not introduce considerable inaccuracies. The predicted ratio between the centerline velocity U_c and the bulk velocity U_b was found to be $U_c/U_b = 1.18$, which is in good agreement with the value of $U_c/U_b = 1.2$ reported by Brandrett and Baines[24] for a higher Reynolds number ($Re_b = 8 \times 10^4$). The magnitude of the maximum secondary velocity is 2.23% of the bulk velocity, which is also in good agreement with the value of 2.20% reported in Ref. 24. In Fig. 11 the normal Reynolds stress profiles along the normal wall bisector are given. The agreement with the experimental data is very

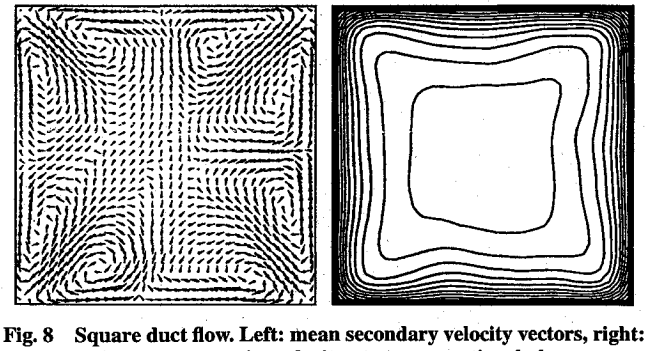

Fig. 8 Square duct flow. Left: mean secondary velocity vectors, right: contours of mean streamwise velocity at a cross-sectional plane.

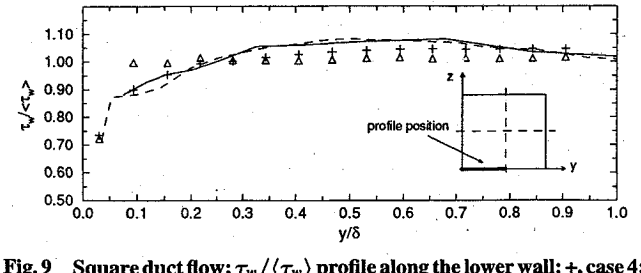

Fig. 9 Square duct flow; $\tau_w/\langle \tau_w \rangle$ profile along the lower wall: +, case 4; △, shifted model; ——, experimental data[27]; and - - -, experimental data.[28]

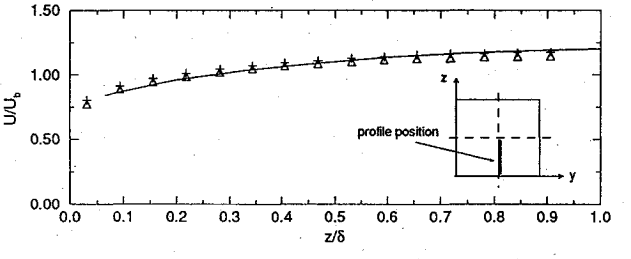

Fig. 10 Square duct flow; mean streamwise velocity profile along the normal wall bisector: +, case 4; △, shifted model; and ——, experimental data.[24]

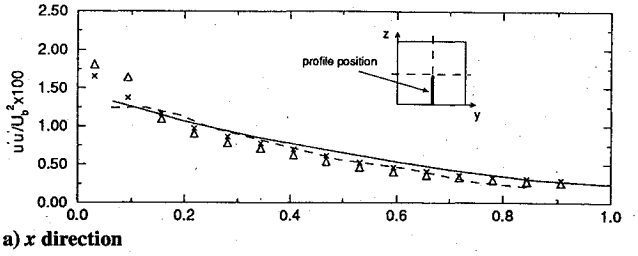

a) x direction

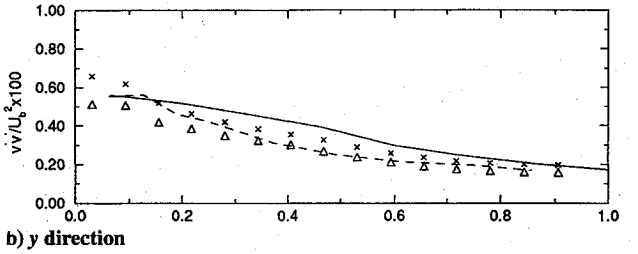

b) y direction

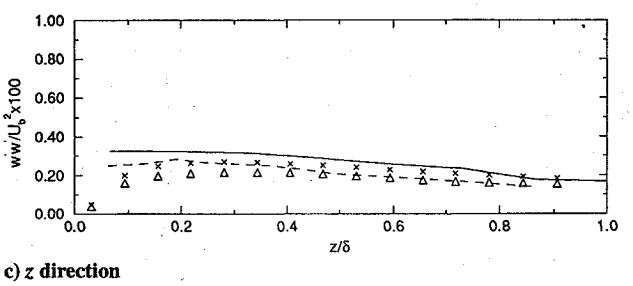

c) z direction

Fig. 11 Square duct flow; turbulence intensities in outer coordinates: ×, case 4; △, shifted model; ——, experimental data[24]; and - - -, experimental data.[25]

good. As for the channel flow case, the influence of the approximate wall boundary condition is restricted to the first few computational points close to the solid boundary, where the proposed model gives a better prediction of all quantities.

C. Rotating Channel Flow Case

System rotation has some important effects on the overall flow structure. It changes the wall-layer streak burst rate and thus modifies the rate of turbulent production, leading to changes in the mean and turbulent flow quantities. The presence of Coriolis forces resulting from the system rotation can either stabilize or destabilize the flow by interacting with the mean shear. On the unstable side turbulence-producing events are enhanced, leading to increased turbulence levels, whereas on the stable side Coriolis forces inhibit production and decrease turbulence levels. These stabilizing/destabilizing effects that appear in the rotating channel make this flow problem a challenging test case for approximate wall boundary conditions. The wall layer dynamics that the model is required to represent are much more complex compared with the zero rotation case.

Three cases were considered for this problem. The rotation rate Ro_b was varied in a range from 0.065 to 0.210 (cases 5–7 in Table 1), while the Reynolds number was kept constant: $Re_\tau = 2 \times 10^2$. The size of the domain was taken equal to $4\pi\delta \times 4/3\pi\delta \times 2\delta$. All computations were started from the zero rotation rate case. Integration in time was continued till a statistical steady state was reached. Statistics were accumulated over 7 nondimensional time units.

In Fig. 12 the predicted friction velocity u_τ normalized by the friction velocity in the absence of rotation $u_{\tau 0}$ is given for all of the rotation rates considered, in comparison with numerical and experimental data available in the literature. The friction velocity agrees well with the resolved LES data in Ref. 29. In general, DNS,[29,30] LES, and experimental[31] data are in good agreement on the unstable side. On the stable side experimental results (dotted-dashed line) are lower than computations (dashed line). A possible reason is the small aspect ratio of the experimental apparatus and the fact that the flow was not fully developed, which may have added a streamwise pressure gradient, increasing the trend of the flow towards relaminarization.[29] The computations of cases 5–7 were repeated using the shifted model, Eqs. (5) and (6). In general, since the model requires the standard law-of-the-wall to be valid, on average it underpredicts the wall stress on the unstable side while it overpredicts the wall stress on the stable side. The error introduced is on the order of 10% for the low rotation rate case (case 5 in Table 1), whereas it increases with increasing rotation rate (approximately 20% for case 7).

The mean velocity profiles are shown in Fig. 13 for all rotation rates considered. The agreement with the resolved LES and DNS data[29] is very good. The influence of the approximate, wall boundary condition is restricted to the first computational point close to the solid boundary. The turbulent intensities are shown in Figs. 14–16. For the low rotation rate case, all quantities are in excellent agreement with the reference data, even in the near-wall region. As the rotation rate increases some discrepancies can be observed for most of the statistics at the stable side of the channel. The reason is probably the different SGS models used in this study and in the resolved LES simulations.[29] The resolved LES data have been obtained with a localized dynamic model that seems to be more appropriate than

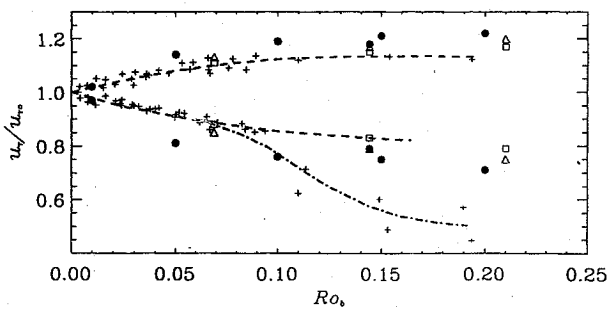

Fig. 12 Rotating channel flow; Friction velocity on unstable and stable sides of the channel: +, experiments[31]; ○, DNS[29,30]; △, resolved LES[29]; and □, present computation $Re_\tau = 200$.

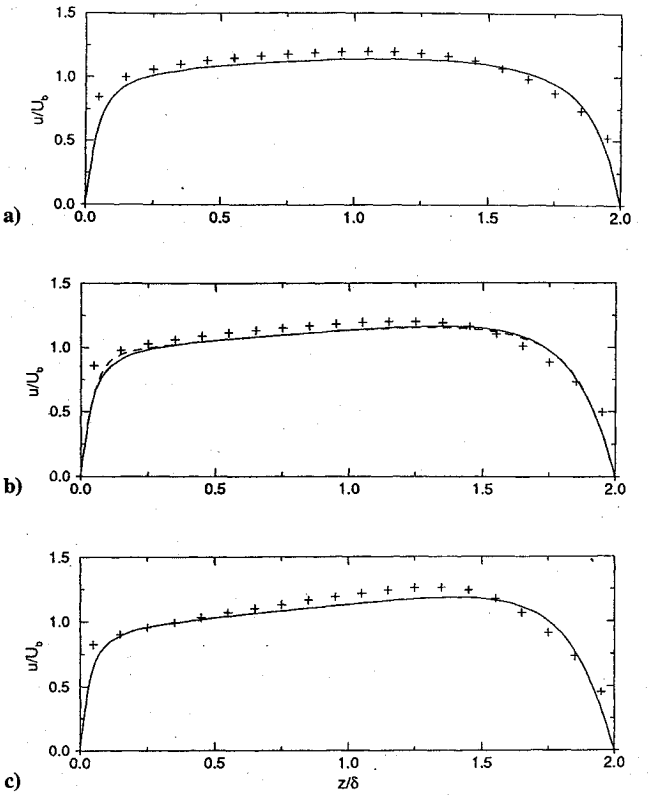

Fig. 13 Rotating channel flow; mean velocity profiles in outer coordinates: a) Ro_b = 0.069: +, case 5; ——, resolved LES[29]; b) Ro_b = 0.144: +, case 6; ——, resolved LES[29]; - - -, DNS[29]; and c) Ro_b = 0.210: +, case 7; ——, resolved LES.[29]

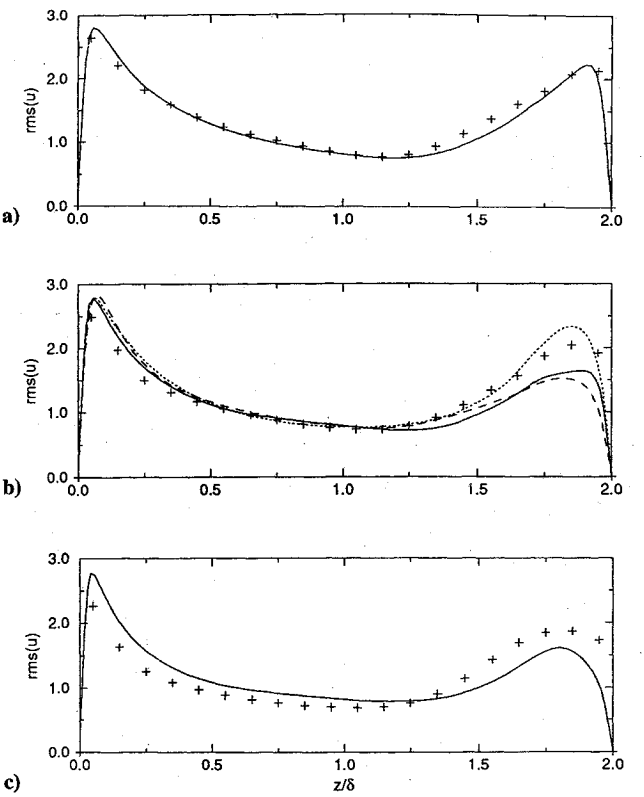

Fig. 14 Rotating channel flow; streamwise turbulence intensities in outer coordinates: Ro_b = 0.069: +, a) case 5; ——, resolved LES[29]; b) Ro_b = 0.144: +, case 6; ——, resolved LES[29]; - - -, DNS[29]; ....., resolved LES plane averaged model[29]; and c) Ro_b = 0.210: +, case 7; and ——, resolved LES.[29]

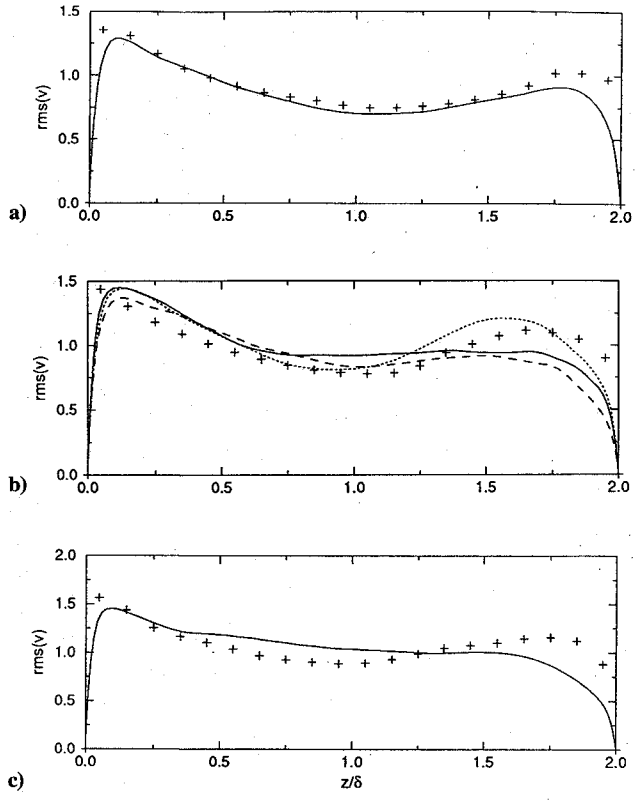

Fig. 15 Rotating channel flow; spanwise turbulence intensities in outer coordinates: a) Ro_b = 0.069: +, case 5; ——, resolved LES[29]; b) Ro_b = 0.144: +, case 6; ——, resolved LES[29]; - - -, DNS[29]; ....., resolved LES plane averaged model[29]; and c) Ro_b = 0.210: +, case 7; and ——, resolved LES.[29]

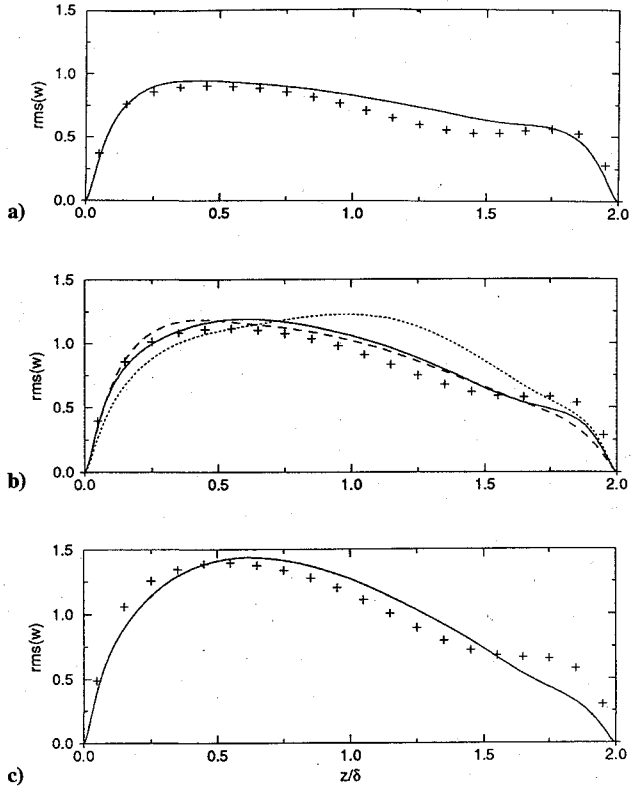

Fig. 16 Rotating channel flow; wall normal turbulence intensities in outer coordinates: a) Ro_b = 0.069: +, case 5; ——, resolved LES[29]; b) Ro_b = 0.144: +, case 6; ——, resolved LES[29]; - - -, DNS[29]; ....., resolved LES plane averaged model[29]; and c) Ro_b = 0.210: +, case 7; ——, resolved LES.[29]

the plane-averaged version used in this study, at the stable side of the channel where intermittent flow regions are present. For $Ro_b = 0.144$ resolved LES data obtained with the plane-averaged model have been added to the graphs. The present data agree well with these results, supporting the preceding line of reasoning.

IV. Concluding Remarks

A new method to model the near-wall region in LES of wall-bounded shear flows is proposed. The model is based on the solution of a simplified set of equations (two-dimensional boundary-layer equations) for each velocity component from the first computational point to the solid boundary. An important feature of this approach is the accurate prediction of the wall shear stress without the additional empirical information required by existing models, such as the existence of a logarithmic layer or additional information on the behavior of the near wall structures.

To investigate the robustness and range of applicability of the proposed model, LES of the flow in a plane channel, a square duct, and a rotating channel have been performed. For all cases the predicted wall shear stress, mean velocities, and turbulent statistics are in very good agreement with numerical and experimental data available in the literature. Improvements for most of the preceding quantities were found in comparison with existing approximate wall boundary conditions, at an additional cost of the order of only 10–15%.

The accuracy of the proposed two-layer treatment in flows with strong and adverse pressure gradients and in separated flows remains to be tested. In such case the use of a more complex set of equations in the near-wall region (for instance, the thin shear layer equations) and a more sophisticated closure (such as, for example, a one-equation model) would be desirable.

Acknowledgments

Financial support for the first author was provided by the European Union under Grant ERBCH-DICT930257. The third author was partially supported by the Office of Naval Research under Grant N0001491J1638, monitored by L. Patrick Purtell.

References

[1]Chapman, D. R., "Computational Aerodynamics Development and Outlook," *AIAA Journal*, Vol. 17, No. 12, 1979, pp. 1293–1313.

[2]Robinson, S. K., "Coherent Motions in the Turbulent Boundary Layer," *Annual Review of Fluid Mechanics*, Vol. 23, 1991, pp. 601–639.

[3]Brooke, J. W., and Hanratty, T. J., "Origin of Turbulence-Producing Eddies in a Channel Flow," *Physics of Fluids A*, Vol. 5, No. 4, 1993, pp. 1011–1022.

[4]Deardorff, J. W., "A Numerical Study of Three-Dimensional Turbulent Channel Flow at Large Reynolds Numbers," *Journal of Fluid Mechanics*, Vol. 41, Pt. 2, 1969, pp. 453–480.

[5]Schumann, U., "Subgrid Scale Model for Finite Difference Simulation of Turbulent Flows in Plane Channel and Annuli," *Journal of Computational Physics*, Vol. 18, No. 4, 1975, pp. 376–404.

[6]Grotzbach, G., "Direct Numerical and Large Eddy Simulation of Turbulent Channel Flows," *Encyclopedia of Fluid Mechanics*, edited by N. P. Cheremisinoff, Gulf Publishing, West Orange, 1987, p. 1337.

[7]Mason, P. J., and Callen, N. S., "On the Magnitude of the Subgrid-Scale Eddy Coefficient in Large-Eddy Simulations of Turbulent Channel Flow," *Journal of Fluid Mechanics*, Vol. 162, Jan. 1986, pp. 439–462.

[8]Piomelli, U., Ferziger, J., Moin, P., and Kim, J., "New Approximate Boundary Conditions for Large Eddy Simulations of Wall-Bounded Flows," *Physics of Fluids A*, Vol. 1, No. 6, 1989, pp. 1061–1068.

[9]Balaras, E., Benocci, C., and Piomelli, U., "Finite Difference Computations of High Reynolds Number Flows Using the Dynamic Subgrid-Scale Model," *Theoretical and Computational Fluid Dynamics*, Vol. 7, No.7, 1995, pp. 207–216.

[10]Bagwell, G., Andrian, R. J., Moser, R. D., and Kim, J., "Improved Approximation of Wall Shear Stress Boundary Conditions for Large Eddy Simulation," *Near Wall Turbulent Flows*, edited by C. G. Speziale and B. P. Launder, Elsevier, Amsterdam, The Netherlands, 1993, pp. 265–275.

[11]Bagwell, G., "Stochastic Estimation of Near Wall Closure in Turbulence Models," Ph.D. Thesis, Dept. of Nuclear Engineering, Univ. of Illinois at Urbana–Champaign, Urbana, IL, 1994.

[12]Naguib, A. M., and Wark, C. E., "An Investigation of Wall-Layer Dynamics Using a Combined Temporal Filtering and Correlation Technique," *Journal of Fluid Mechanics*, Vol. 243, Oct. 1992, p. 541.

[13]Piomelli, U., "High Reynolds Number Calculations Using the Dynamic Subgrid-Scale Stress Model," *Physics of Fluids A*, Vol. 5, No. 6, 1993, pp. 1484–1490.

[14]Germano, M., Piomelli, U., Moin, P., and Cabot, W. H., "A Dynamic Subgrid-Scale Eddy Viscosity Model," *Physics of Fluids A*, Vol. 3, No. 7, 1991, pp. 1760–1765.

[15]Smagorinsky, J., "General Circulation Experiments with the Primitive Equations, I. The Basic Experiment," *Monthly Weather Review*, Vol. 91, 1963, p. 99.

[16]Lilly, D. K., "A Proposed Modification of the Germano Subgrid-Scale Closure Method," *Physics of Fluids A*, Vol. 4, No. 3, 1992, pp. 633–635.

[17]Schmidt, H., Schumann, U., and Volkert, H., "Three-Dimensional, Direct and Vectorized Elliptic Solvers for Various Boundary Conditions, DFVLR, TR DFVLR-mitt. 84-15, Köln, Germany, July 1984.

[18]Kim. J., Moin, P., and Moser, R., "Turbulent Statistics in Fully Developed Channel Flow at Low Reynolds Number," *Journal of Fluid Mechanics*, Vol. 177, April 1987, pp. 133–166.

[19]Balint, J. L., Wallace, J. M., and Vukoslavcevic, P., "The Velocity and Vorticity Fields of a Turbulent Boundary Layer. Part 2. Statistical Properties," *Journal of Fluid Mechanics*, Vol. 228, 1991, pp. 53–86.

[20]Mansour, N. N., Kim, J., and Moin, P., "Reynolds-Stress and Dissipation-Rate Budgets in a Turbulent Channel Flow, *Journal of Fluid Mechanics*, Vol. 194, 1988, pp. 15–44.

[21]Iacovides, H., and Launder, B. E., "ASM Predictions of Turbulent Momentum and Heat Transfer in Coils and U-Bends," *International Conference on Numerical Methods in Laminar and Turbulent Flow*, edited by C. Taylor, M. D. Olson, P. M. Gresho, and W. G. Habashi, Pineridge, Swansea, Wales, UK, 1985, pp. 1023–1045.

[22]Launder, B. E., "An Introduction to Single-Point Closure Methodology," *An Introduction to the Modeling of Turbulence*, von Kármán Inst. Lecture Series 91-02, von Kármán Inst., Brussels, Belgium, 1991.

[23]Speziale, C. G., "The Dissipation Rate Correlation and Turbulent Secondary Flows in Non-Circular Ducts," *Journal of Fluids Engineering*, Vol. 108, 1986, pp. 118–120.

[24]Brundrett, E., and Baines, W. D., "The Production and Diffusion of Vorticity in a Duct Flow," *Journal of Fluid Mechanics*, Vol. 19, Pt. 3, 1964, pp. 375–394.

[25]Gessner, F. B., "The Origin of Secondary Flow in Turbulent Flow Along a Corner," *Journal of Fluid Mechanics*, Vol. 58, Pt. 1, 1973, pp. 1–25.

[26]Gavrilakis, S., "Numerical Simulation of Low Reynolds Number Turbulent in a Straight Duct," *Journal of Fluid Mechanics*, Vol. 244, Nov. 1993, pp. 101–129.

[27]Lund, E. G., "Mean Flow and Turbulence Characteristics in the Near Corner Region of a Square Duct," M.S. Thesis, Dept. of Mechanical Engineering, Univ. of Washington, Seattle, WA, 1977.

[28]Leutheusser, H. J., "Turbulent Flow in Rectangular Ducts," *Journal of the Hydraulics Division*, Vol. 89, No. HY3, 1963, pp. 1–19.

[29]Piomelli, U., and Liu, J., "Large Eddy Simulation of Rotating Channel Flows Using a Localized Dynamic Model," *Physics of Fluids*, Vol. 7, No. 4, 1995, pp. 839–848.

[30]Kristofferesen, R., and Andersson, H. I., "Direct Simulation of Low Reynolds Number Turbulent Flow in a Rotating Channel," *Journal of Fluid Mechanics*, Vol. 256, Nov. 1993, p. 163.

[31]Johnston, J. P., Halleen, R. M., and Lezius, D. K., "Effects of Spanwise Rotation on the Structure of Two-Dimensional Fully Developed Turbulent Channel Flow," *Journal of Fluid Mechanics*, Vol. 56, Pt. 3, 1972, p. 533.